


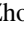



Structure and decay mechanism of the low-lying states in ${}^9\text{Be}$ and ${}^9\text{B}$

Y. H. Yang (杨依豪) ^{1,2,3} Y. G. Ma (马余刚) ^{3,4,*} S. M. Wang (王思敏) ^{3,4,†}
B. Zhou (周波) ^{3,4} and D. Q. Fang (方德清) ^{3,4}

¹Shanghai Institute of Applied Physics, Chinese Academy of Sciences, Shanghai 201800, China

²University of Chinese Academy of Sciences, Beijing 100049, China

³Key Laboratory of Nuclear Physics and Ion-beam Application (MOE), Institute of Modern Physics, Fudan University, Shanghai 200433, China

⁴Shanghai Research Center for Theoretical Nuclear Physics, NSFC and Fudan University, Shanghai 200438, China



(Received 28 February 2023; revised 12 August 2023; accepted 25 September 2023; published 11 October 2023)

Background: As a Borromean system, ${}^9\text{Be}$ is weakly bound, while its mirror partner ${}^9\text{B}$ is an unbound system. Such weakly bound and unbound nuclei are usually accompanied with exotic structures and decay modes which attract a lot of experimental and theoretical attentions.

Purpose: Due to the mirror symmetry, ${}^9\text{B}$ and ${}^9\text{Be}$ share many similar properties, but experience different continuum effect mainly caused by Coulomb interaction. In this work, we try to gain more insight into the cluster structures of ${}^9\text{B}$ and ${}^9\text{Be}$, and analyze the Thomas-Ehrman effect therein. Meanwhile, another purpose of this work is to study the decay dynamics and mechanisms of ${}^9\text{Be}$ and ${}^9\text{B}$, and explore the possible three-body decay in their low-lying states.

Methods: The three-body Gamow coupled-channel method has been used to calculate the structures of ${}^9\text{Be}$ and ${}^9\text{B}$ mirror systems. The corresponding wave functions have been propagated to analyze the decay dynamics.

Results: According to the calculated spectra and density distributions of ${}^9\text{Be}$ and ${}^9\text{B}$, the Thomas-Ehrman effect is found in those states with small orbital-angular momenta. By comparing the wave functions in two- and three-body frameworks, the nature of the $1/2^+$ state of ${}^9\text{Be}$ has been discussed. Moreover, the low-lying states with possibly different decay mechanisms have been discussed based on the results of the density evolution and asymptotic correlations.

Conclusions: Consequently, it has been found that the behavior of the two-body virtual state can leave an imprint in a many-body system, but its characteristics might be diluted by the configuration mixing especially for the nuclei with two subsystems unbound. As to the decay properties, it has been demonstrated that ${}^9\text{Be}(5/2^+)$, ${}^9\text{Be}(1/2^+)$, and ${}^9\text{B}(5/2^-)$ are likely to correspond to the sequential, “democratic”, and three-body decay mechanisms, respectively.

DOI: [10.1103/PhysRevC.108.044307](https://doi.org/10.1103/PhysRevC.108.044307)

I. INTRODUCTION

${}^9\text{Be}$ is a typical nucleus with cluster structure. Its components $\alpha + \alpha + n$ form a Borromean system [1], in which none of the two-body subsystems (either ${}^8\text{Be}$ or ${}^5\text{He}$) is bound [2,3]. Therefore, it attracts extensive studies [4–8]. From the theoretical side, various models have been used to focus on different aspects of the system, including cluster models [9–15], antisymmetrized molecular dynamics [16–19], microscopic multicluster model [20,21], projected Hartree-Fock [22], shell model [23,24], quantum Monte Carlo [25], *ab initio* no-core shell model [26] as well as an extended quantum molecular dynamics model which enables to describe α -cluster states [27–29]. However, there are still large uncertainties in the structural and decay properties of the low-lying excited states.

In particular, the nature of the first excited state $1/2^+$ in ${}^9\text{Be}$ is still under debate. It is believed to be a virtual (antibound) state within the two-body (${}^8\text{Be} + n$) framework [20,30,31], while a normal resonance in the three-body ($\alpha + \alpha + n$) model [32–34] or other many-body methods [16–19,25,26]. Experimentally, a near-threshold state has been measured with a relatively large decay width [35]. However, it is difficult to distinguish a scattering feature from a proper resonance through spectrum or cross-section analysis [36]. To this end, we aim to gain some insights into this state, and investigate some general properties of a virtual state in the many-body medium.

Another interesting aspect regarding to the excited states of ${}^9\text{Be}$ is the decay mechanism. Due to the unbound nature of ${}^8\text{Be}$ and ${}^5\text{He}$, the excited states of ${}^9\text{Be}$ could shed light on the features of its constituent clusters by two single α s and n , or prompt 2α decays and n . The former corresponds to a sequential mode, while the latter is a three-body process. Figuring this out would help us better understand the inner structure and corresponding nucleosynthesis process [6,37].

*mayugang@fudan.edu.cn

†wangsimin@fudan.edu.cn

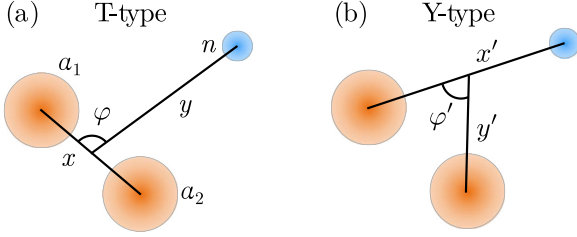


FIG. 1. The schematic figure for three-body $\alpha + \alpha + n$ system in Jacobi- T (a) and Jacobi- Y (b) coordinates.

So far, such kind of three-particle decay has mainly been directly observed in a handful of proton-rich nuclei [38–45], and is known as the two-proton ($2p$) decay. Also, there are some candidates in some neutron-rich systems [46–50]. In this work, we are trying to figure out whether the three-body decay exists in the system whose constituent components are clusters.

To figure out the decay properties, particle correlation that can be directly measured would be an important tool. It provides valuable information on the emitted particles, and has been widely used to determine the decay mechanism of $2p$ emission [38]. Meanwhile, the correlations of the emitted two α particles have been measured in the $5/2^-$ state of ${}^9\text{B}$ [51], although it is not clear yet about the corresponding decay mechanism. Noticing that ${}^9\text{Be}$ and ${}^9\text{B}$ are mirror nuclei with proton and neutron numbers exchanged, studying the properties of ${}^9\text{Be}$ would be helpful to understand the structure and decay of ${}^9\text{B}$. Due to the different Coulomb interaction and continuum effects, it is also interesting to investigate isospin symmetry breaking and Thomas-Ehrman shift [52–56] between this mirror pair. Moreover, in this work, we utilize a time-dependent approach to figure out the connection between the asymptotic correlation and the inner structure.

This article is organized as follows. Section II describes the model and parameters used in this work. In Sec. III, we show the results of the energy spectra, density distributions, time-dependent evolutions, and particle correlations of the ${}^9\text{Be}$ - ${}^9\text{B}$ mirror pair. Finally, the summary and outlook are provided in Sec. IV.

II. THE MODEL

A. Gamow coupled-channel approach

In this work, a Gamow coupled-channel (GCC) approach [57] is used, which is a three-body model in which the nucleus is described in terms of two α clusters and a valence nucleon. The i th cluster ($i = \alpha_1, \alpha_2, n$) has a position vector \vec{r}_i and linear momentum \vec{k}_i . To properly describe the three-body asymptotic behavior, the wave function can be expressed in Jacobi (relative) coordinates:

$$\begin{aligned}\vec{x} &= \sqrt{\mu_x}(\vec{r}_{i_1} - \vec{r}_{i_2}), \\ \vec{y} &= \sqrt{\mu_y} \left(\frac{A_{i_1}\vec{r}_{i_1} + A_{i_2}\vec{r}_{i_2}}{A_{i_1} + A_{i_2}} - \vec{r}_{i_3} \right),\end{aligned}\quad (1)$$

where $i_1 = \alpha_1, i_2 = \alpha_2, i_3 = n$ for the T coordinate and $i_1 = n, i_2 = \alpha_1, i_3 = \alpha_2$ for the Y coordinate, see Fig. 1. In Eq. (1)

A_i is the i th cluster mass number, and $\mu_x = \frac{A_{i_1}A_{i_2}}{A_{i_1} + A_{i_2}}$ and $\mu_y = \frac{(A_{i_1} + A_{i_2})A_{i_3}}{A_{i_1} + A_{i_2} + A_{i_3}}$ are the reduced masses associated with \vec{x} and \vec{y} , respectively. In practice, it is convenient to introduce hyper-radius $\rho = \sqrt{x^2 + y^2}$, which is transformation-invariant among different sets of Jacobi coordinates.

Since the experimental measurements are done in the momentum space, one defines the relative momenta

$$\begin{aligned}\vec{k}_x &= \mu_x \left(\frac{\vec{k}_{i_1}}{A_{i_1}} - \frac{\vec{k}_{i_2}}{A_{i_2}} \right), \\ \vec{k}_y &= \mu_y \left(\frac{\vec{k}_{i_1} + \vec{k}_{i_2}}{A_{i_1} + A_{i_2}} - \frac{\vec{k}_{i_3}}{A_{i_3}} \right),\end{aligned}\quad (2)$$

where θ_k and θ'_k are the opening angles of (\vec{k}_x, \vec{k}_y) in Jacobi- T and Jacobi- Y coordinates, respectively. $E_{\alpha\alpha} = \frac{\hbar^2 k_x^2}{2\mu_x}$ is the kinetic energy of the relative motion of the emitted two α particles and $E_{\alpha n}$ is that of the α -neutron pair.

The total wave function of the parent nucleus is written as

$$\Psi^{J\pi} = \rho^{-5/2} \sum_{\gamma, K} C_{\gamma K}(k) \mathcal{B}^{\gamma K}(k, \rho) \mathcal{Y}_{\gamma K}^{JM}(\Omega) dk, \quad (3)$$

where $\mathcal{Y}_{\gamma K}^{JM}(\Omega)$ is the hyperspherical harmonics for the hyperangle part, K is the hyperspherical quantum number, and $\gamma = \{\ell_x, \ell_y, L\}$, where ℓ is the orbital-angular momentum in the corresponding Jacobi- T coordinate. For example, in the Jacobi- T coordinate, ℓ_x is the orbital-angular momentum of the α - α pair with respect to their center of mass, while ℓ_y is the pair's orbital-angular momentum with respect to the nucleon. k is the total momentum defined as $\sqrt{k_x^2/\mu_x + k_y^2/\mu_y}$. Equation (3) takes the integral over continuous k (scattering states) and the sum over γ, K , and discretized k (bound and decaying resonant states). The hyper-radial part is expanded in the Berggren ensemble that defines a complete basis $\mathcal{B}_n^{\gamma K}(\rho)$ in the complex-momentum k plane including bound, decaying, and scattering states [57–59]. Because of the inherent symmetry within the Berggren basis [58], scattering states are selected by the momentum k along a contour \mathcal{L}^+ in the fourth quadrant of the complex plane. This indicates that the wave function exclusively incorporates the outgoing k momentum components, while disregarding the conjugate momenta. The Berggren basis does not belong to the Hilbert space, so the mathematical apparatus of quantum mechanics in Hilbert space is inadequate [58,60]. Consequently, the mathematical structure of the rigged Hilbert space (RHS) [61,62] can accommodate time-asymmetric processes, such as particle decays, by extending the domain of quantum mechanics. This yields a different inner product for these single-particle states in the complex plane, and it is able to show that they are orthogonal and normalizable to

$$\langle \tilde{\mathcal{B}}_i | \mathcal{B}_j \rangle = \int_0^\infty \mathcal{B}(k_i, \rho) \mathcal{B}(k_j, \rho) d\rho = \delta(k_i - k_j). \quad (4)$$

The tilde symbol above bra vector $\langle \tilde{\mathcal{B}}_i |$ is the time-reversed operator, which signifies the complex conjugation arising in the dual space. By using the Berggren basis, the inner and

asymptotic regions of the Schrödinger equation can be treated on the same footing, and this provides the natural connection between nuclear structure and decay aspects of the problem.

The Hamiltonian in the three-body GCC model can be written as

$$\hat{H} = \sum_{i=1}^3 \frac{\hat{p}_i^2}{2m_i} + \sum_{i=1}^2 V_{\alpha n}(\xi_i) + V_{\alpha\alpha} - \hat{T}_{c.m.}, \quad (5)$$

where $\hat{p}_i^2/(2m_i)$ and $\hat{T}_{c.m.}$ are kinetic operators for each particle and the center of mass of the system, respectively. In Jacobi coordinates, the center of mass is automatically eliminated. $V_{\alpha n}$ and $V_{\alpha\alpha}$ are pairwise interactions for $\alpha - n$ and $\alpha - \alpha$ particles, respectively.

In order to deal with the antisymmetrization between $\alpha - \alpha$ and $\alpha - n$, we used the supersymmetric transformation method [63–65], which introduces an auxiliary repulsive “Pauli core” in the original interaction to eliminate Pauli-forbidden states. The Pauli principle between clusters is satisfied by introducing a global principal quantum number G , which can be estimated by the Wildermuth rule [66–68],

$$G = 2N + L = \sum_{i=1}^{A_c} g_i, \quad g_i = 2n_i + \ell_i, \quad (6)$$

where g_i represent the principal quantum number of the cluster-nucleon orbit located above the Fermi level, and A_c is the number of the nucleons inside the cluster. N and L are the node number and orbital-angular momentum in the radial wave function of the cluster motion, respectively, while n and ℓ correspond to those of the nucleons inside the cluster. Consequently, $G \geq 4$ for the $\alpha + \alpha$ [69] subsystem, while $G \geq 1$ for $\alpha + n$.

The Gamow state $\Psi^{J\pi}$ is obtained by diagonalizing the complex-symmetric Hamiltonian. This state exhibits purely outgoing wave asymptotics and is associated with a complex energy $\bar{E} = E_r - i\Gamma/2$, where Γ represents the decay width, defining the half-life of the system. Similar to the single-particle basis, $\Psi^{J\pi}$ can be normalized as follows [59,70]:

$$\langle \tilde{\Psi}^{J\pi} | \Psi^{J\pi} \rangle = 1, \quad (7)$$

where $\tilde{\Psi}^{J\pi}$ is the time-reversed many-body state. This normalization can be achieved using the complex scaling method [71,72] or by verifying that the expansion coefficients satisfy $\sum \int C_{\gamma K}^2(k) dk = 1$. As a result, the observables in this framework are also complex, with their imaginary parts representing the uncertainty. For instance, one can define the complex density distribution as follows:

$$\rho_c = \langle \tilde{\Psi}^{J\pi} | \delta(r_x - R_{\alpha-\alpha}) \delta(r_y - R_{2\alpha-n/p}) | \Psi^{J\pi} \rangle, \quad (8)$$

where $r_x = x/\sqrt{\mu_x}$ and $r_y = y/\sqrt{\mu_y}$. Here, $R_{\alpha-\alpha}$ represents the distance between two α particles, and $R_{2\alpha-n/p}$ denotes the distance between the α pair and the valence nucleon.

B. Time-dependent approach

To analyze the decay dynamics of the excited ${}^9\text{Be} - {}^9\text{B}$ mirror systems and investigate the correlations of the emitted α particles, a time-dependent approach is necessary [46,73].

Starting with the resonance wave function obtained from the complex GCC framework, we decompose it into real-momentum scattering states using the Fourier-Bessel series expansion in the real-energy Hilbert space [74]. The resulting wave packet $\Psi_0^{J\pi}$ serves as the initial state. The wave function $\Psi_t^{J\pi}$ at time t can be obtained by propagating $\Psi_0^{J\pi}$ through the time evolution operator $\exp(-i\hat{H}t/\hbar)$ [73,75]. To maintain the Hermitian property of the Hamiltonian matrix and ensure conservation of the total density, we limit the time evolution to the real momentum space, resulting in a real calculated density distribution ρ_r . At time t , the density distribution can be expressed as

$$\rho_r(t) = \langle \Psi_t^{J\pi} | \delta(r_x - R_{\alpha-\alpha}) \delta(r_y - R_{2\alpha-n/p}) | \Psi_t^{J\pi} \rangle. \quad (9)$$

The wave function encompasses all the configurations during the time evolution, making it possible to investigate structural changes at different time points throughout the decay process.

C. Hamiltonian and parameters

For the three-body ($\alpha + \alpha + n$) GCC Hamiltonian, we used the same potentials for $V_{\alpha n}$ and $V_{\alpha\alpha}$ as Ref. [76], and excluded the state-dependent three-body force. In details, the $\alpha - n$ interaction $V_{\alpha n}$ is given by the KKNN potential [77]. In the case of ${}^9\text{B}$, an additional Coulomb potential with a dilatation-analytic form ($R_c = 2\text{ fm}$) is added for $V_{\alpha p}$. The $\alpha - \alpha$ interaction $V_{\alpha\alpha}$ (including Coulomb interaction) is taken from Ref. [31] originating from a folding potential of the effective NN interaction [78]. For comparison, ${}^9\text{Be}$ is also studied in the two-body framework, in which the effective ${}^8\text{Be} + n$ Hamiltonian is described by a Woods-Saxon (WS) potential with parameters as Ref. [30]. The resulting energy for the $1/2^+$ virtual state is -0.119 MeV .

The three-body calculations have been carried out in the model space of $\max(\ell_x, \ell_y) \leq 8$ with the maximal hyper-spherical quantum number $K_{\max} = 16$. For the hyper-radial part, we used the Berggren basis for the $K \leq 4$ channels and the harmonic oscillator (HO) basis for the higher-angular momentum channels. The complex-momentum contour of the Berggren basis is defined as $k = 0 \rightarrow 0.3 - 0.12i \rightarrow 0.4 - 0.06i \rightarrow 0.5 \rightarrow 0.8 \rightarrow 1.2 \rightarrow 2 \rightarrow 4$ (all in fm^{-1}) with each segment discretized with 35 points. For the HO basis we took the oscillator length $b = 1.75\text{ fm}$ and $N_{\max} = 50$. To obtain the virtual state in the two-body framework, we used same model space but with a deformed contour for the Berggren basis, which is $k = 0 \rightarrow -0.1 \rightarrow 0 - 0.2i \rightarrow 0.3 - 0.1i \rightarrow 0.4 - 0.05i \rightarrow 0.5 \rightarrow 0.8 \rightarrow 1.2 \rightarrow 2 \rightarrow 4$ (all in fm^{-1}).

For time-dependent evolution, the inner part ($< 15\text{ fm}$) of the initial state is expanded and propagated with a real-momentum contour, which is $k = 0 \rightarrow 0.225 \rightarrow 0.3 \rightarrow 0.375 \rightarrow 0.45 \rightarrow 1.2 \rightarrow 6$ (all in fm^{-1}), and each segment is discretized with 90 scattering states. For the hyper-radial part, we used the Berggren basis for the $K \leq 6$ channels for a better description of the farther radius. In practice, the interactions inside the sphere of radius 400 fm are considered. The other model space parameters are the same as above.

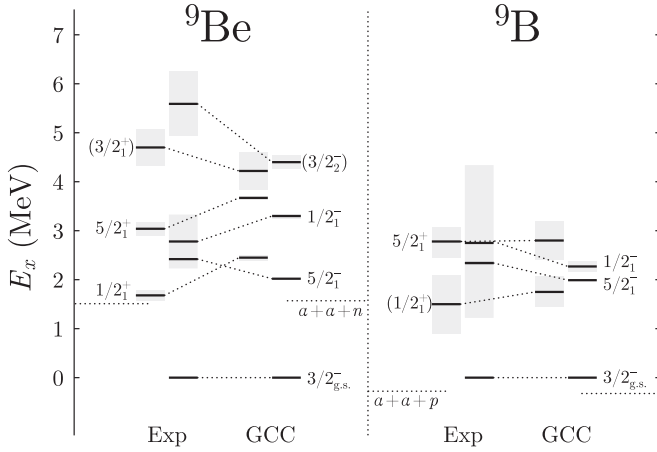


FIG. 2. Calculated spectra and decay widths (shaded areas) of the ${}^9\text{Be}$ - ${}^9\text{B}$ pair. Also shown are the experimental data taken from Refs. [79,80].

III. RESULTS AND DISCUSSIONS

A. Structure information of ${}^9\text{Be}$ and ${}^9\text{B}$

In our framework, the difference of this mirror pair is the existing Coulomb interaction between the α particle and the valence nucleon. To better understand the interplay between the Coulomb and nuclear interactions, the structural and decay properties of the ${}^9\text{Be}$ - ${}^9\text{B}$ mirror pair have been compared. Due to the isospin symmetry between the proton and neutron, the mirror nuclei pairs have similar properties in most aspects [81–84]. However, the presence of the Coulomb interaction makes ${}^9\text{Be}$ and ${}^9\text{B}$ have different thresholds. The former is particle bound with the neutron separation energy $S_n = 1.665$ MeV, while the latter is unbound with $S_p = -0.186$ MeV [85]. Consequently, this results in different continuum effects, which would manifest themselves in the spectra, density distributions, and decay mechanism.

As shown in Fig. 2 and Table I, the calculated spectra of ${}^9\text{Be}$ and ${}^9\text{B}$ are in agreement with experimental values qualitatively. Due to the lack of data, the spin-parities of some states have not been determined yet [86], which can be estimated based on the mirror symmetry and the calculated energy spectra (see the spin assignments in Fig. 2). The first excited state of ${}^9\text{B}$ has been studied by Refs. [87–90]

attempting to predict its value using the Thomas-Ehrman shift [52,53]. In detail, Ref. [88] expanded the study of Ref. [89] by investigating how different nuclear numbers A affect the magnitude of the Thomas-Ehrman shift in light nuclei. The prediction suggested that the energy difference between $1/2_1^+$ and $5/2_1^+$ in ${}^9\text{B}$ would be slightly smaller than that in ${}^9\text{Be}$, which aligns with experimental results and our calculations. Also, the $J^\pi = 1/2_1^+$ and $5/2_1^+$ states in both ${}^9\text{Be}$ and ${}^9\text{B}$ have relatively low excitation energies, which indicates that a cluster dipole mode ($\Delta L = 1$ related to the $3/2_1^-$ g.s.) would be possible near the threshold [91]. Moreover, a Thomas-Ehrman shift occurs between the analog states, particularly in those ($J^\pi = 1/2_1^+$ and $1/2_1^-$) with relatively low- ℓ orbitals. It is because these orbitals (s or p wave) have smaller centrifugal barriers, and could experience more continuum.

This can be also seen in the density distributions. In Fig. 3, we present the predicted density distributions in Jacobi coordinates for the low-lying states of ${}^9\text{Be}$ and ${}^9\text{B}$. Based on the definitions of Eqs. (8), (9), the densities, denoted by ρ_c and ρ_r , represent the initial states ($t = 0$) in rigged Hilbert and Hilbert spaces, respectively, and are calculated using the complex GCC framework and time-dependent approach. Inside the nucleus, both ρ_r and $\text{Re}(\rho_c)$ exhibit striking similarities, indicating that the structural information of the atomic nucleus primarily manifests itself in the real part of ρ_c , while the imaginary part mainly resides outside the nucleus, representing the decay process and uncertainty. For bound or quasibound states, $\text{Im}(\rho_c)$ can be neglected. However, as the decay width increases, the contribution of $\text{Im}(\rho_c)$ becomes more pronounced. Since our focus is on studying the decay dynamics and structural evolution using the time-dependent approach, the density distributions are limited to the Hilbert space in subsequent discussions and figures.

Comparing the densities of ${}^9\text{Be}$ and ${}^9\text{B}$ mirror systems, we find that the $J^\pi = 3/2_{g.s.}^-$ and $5/2_1^-$ states are quasilocalized due to their low energies or high- ℓ orbitals. This observation is further supported by the negligible proportion of the imaginary part in the density distribution. These mirror nuclei exhibit similar structures, where three components form a triangular configuration, as depicted in Fig. 3. Meanwhile, other states with densities widely distributed are more easily impacted by the nonlocalized scattering continuum, which results in different structures between the proton- and neutron-rich sides. Taking the $1/2_1^-$ state as an example, according to

TABLE I. Calculated spectra and decay widths (all in MeV) of the ${}^9\text{Be}$ - ${}^9\text{B}$ mirror pair. The energies are with respect to the ground state (g.s.) of ${}^8\text{Be}$. Also shown are the experimental data taken from Refs. [79,80]

J^π	${}^9\text{Be}$		${}^9\text{B}$	
	$E_{\text{Exp.}}(\Gamma_{\text{Exp.}})$	$E_{\text{GCC}}(\Gamma_{\text{GCC}})$	$E_{\text{Exp.}}(\Gamma_{\text{Exp.}})$	$E_{\text{GCC}}(\Gamma_{\text{GCC}})$
$3/2_{g.s.}^-$	-1.66	-1.51	0.19(5.4×10^{-4})	0.32(5.2×10^{-6})
$1/2_1^+$	0.02(0.21)	0.94(0.11)	1.69(1.20)	2.06(0.63)
$5/2_1^-$	0.76(7.8×10^{-4})	0.51(1.9×10^{-6})	2.53(0.08)	2.31(4.4×10^{-3})
$1/2_1^-$	1.12(1.10)	1.79(0.09)	2.97(3.13)	2.59(0.21)
$5/2_1^+$	1.38(0.28)	2.16(0.08)	2.94(0.61)	3.12(0.78)
$3/2_1^+$	3.04(0.74)	2.71(0.76)		
$3/2_2^-$	3.93(1.33)	2.89(0.28)		

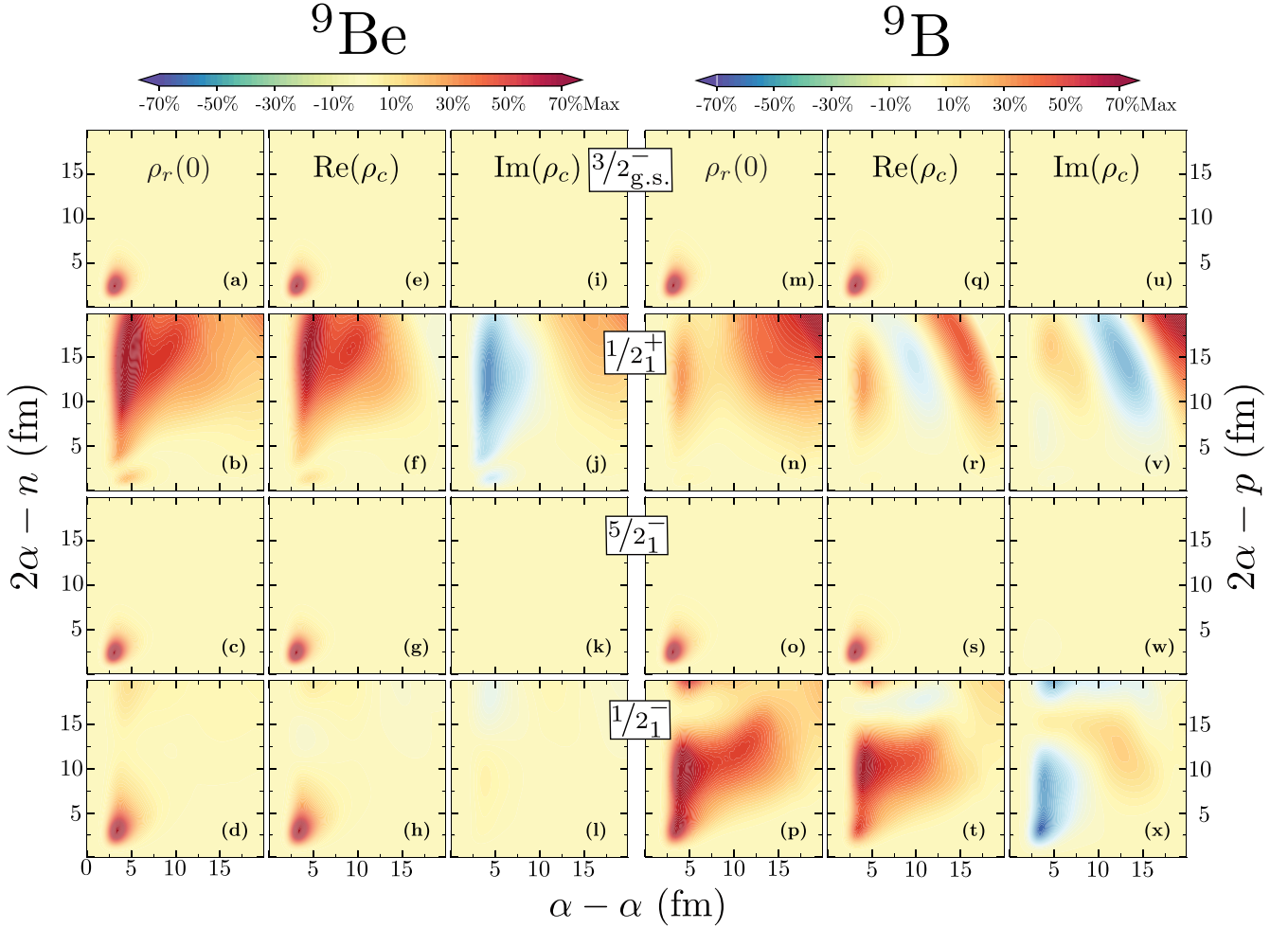


FIG. 3. Predicted density distributions (in fm^{-2}) in Jacobi coordinates for low-lying states ${}^9\text{Be}$ (left) and ${}^9\text{B}$ (right). ρ_r and ρ_c are density distributions of the initial states ($t = 0$) in Hilbert and rigged Hilbert spaces, respectively. See Eqs. (8), (9) and the corresponding discussions for the details.

the calculation of GCC, ${}^9\text{Be}$ is dominated by the triangular configuration, while ${}^9\text{B}$ has another primary component that represents the ${}^8\text{Be} + p$ configuration. In this component, the two α particles are spatially close, and the α - α pair is relatively distant from the valence proton. A similar situation occurs in the $1/2_1^+$ state. As shown in Fig. 3, although the $1/2_1^+$ state is close to the threshold, the particle density is pretty low inside the nucleus, and the primary component clearly forms ${}^8\text{Be} + n$ configuration. This is in accord with the behavior of the virtual state that the relative motion between the valence neutron and the core (${}^8\text{Be}$) is governed by an s wave. As to ${}^9\text{B}$, there is also a similar ${}^8\text{Be} + p$ configuration, but the presence of the repulsive Coulomb interaction makes the components of the system more favorable to be apart from each other.

To gain more insight into the nature of this $1/2_1^+$ state of ${}^9\text{Be}$, the overlap functions between ${}^9\text{Be}$ and ${}^8\text{Be}$ (g.s.) have been calculated in both three- and two-body frameworks (see Fig. 4), which represent the relative motion between the valence neutron and ${}^8\text{Be}$. Similar to the density distribution, normally, the overlap function between bound or quasibound

states is mainly located inside the nucleus, which is the case for the g.s. of ${}^9\text{Be}$ and ${}^8\text{Be}$. When dealing with a resonance, the overlap function in the asymptotic region is proportional to the Hankel or Coulomb wave function. This manifests itself as the divergently asymptotic behavior in Hilbert space and relatively large imaginary components in the RHS as shown in Figs. 4(a) and 4(b), respectively. In particular, for a virtual state, there is only a little amount of overlap function trapped within the space of the nuclear radius as shown in the overlap function for the $1/2_1^+$ state by the two-body framework (see Fig. 4). Thus, it is also known as the antibound state.

When going beyond two-body degrees of freedom, the situation is a little bit more complicated. As shown in Fig. 4(a), due to the different treatments of the Pauli principle, the short-range (< 5 fm) overlap function for the $1/2_1^+$ state in the three-body framework is slightly different from that in the two-body framework. In the mid-range, both overlap functions are in good agreement, which manifests themselves as the behavior of a virtual state. However, the discrepancy becomes larger and larger when the distance increases. This is due to the fact that the g.s. of ${}^8\text{Be}$ is not stable, and will be

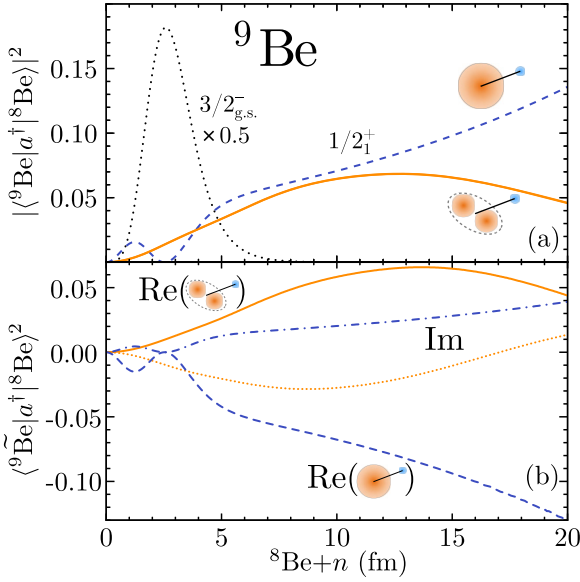


FIG. 4. (a) The squared norm overlap function between ${}^9\text{Be}$ ($\alpha + n$) and ${}^8\text{Be}$ ($\alpha + \alpha$) g.s. predicted by GCC in Hilbert space. The wave function of ${}^8\text{Be}$ and ${}^9\text{Be}$ is described as $\alpha + \alpha$ and $\alpha + \alpha + n$, respectively. The dotted and solid lines correspond to the $3/2^-$ g.s. and $1/2_1^+$ excited state of ${}^9\text{Be}$, respectively, while the dashed line shows the result for the $1/2_1^+$ state within the two-body framework (${}^8\text{Be} + n$). (b) The real (solid and dashed lines) and imaginary (dotted and dash-dotted lines) parts of the squared overlap function (rigged Hilbert space) for the $1/2_1^+$ excited state of ${}^9\text{Be}$.

split into two α particles without the interaction of the extra neutron. Consequently, when the valence neutron of ${}^9\text{Be}$ is far from the ${}^8\text{Be}$, the two-body (${}^8\text{Be} + n$) system begins to fall apart, and the behavior of virtual state cannot be held any more. This indicates that, in the many-body cases, a certain configuration (channel) would manifest itself as the behavior of the virtual state, but due to the configuration mixing, part of its characteristics might be diluted. Although it is impossible for a virtual state to emerge in proton-rich nuclei due to the Coulomb interaction [54], the analog state in ${}^9\text{B}$ has a widely distributed density and relatively large decay width, which is located around the region of threshold and subthreshold resonance. Hence, these states would be interesting for further experimental and theoretical investigations.

B. Decay properties of ${}^9\text{Be}$ and ${}^9\text{B}$

As discussed above, the low-lying states of ${}^9\text{Be}$ and ${}^9\text{B}$ contain different components and densities. Although such structural information is hard to measure directly, it leaves a strong imprint on the decay properties. To this end, in this section, we try to analyze the decay dynamics and possible three-body mechanism of the low-lying states of ${}^9\text{Be}$ and ${}^9\text{B}$, in which we have selected typical cases for discussion. As discussed earlier, the time-dependent framework is restricted to the real-energy Hilbert space, leading to real-valued density distributions and other observables. In this context, all the quantities obtained from our calculations, including density distributions, are inherently real due to the limitations of the approach.

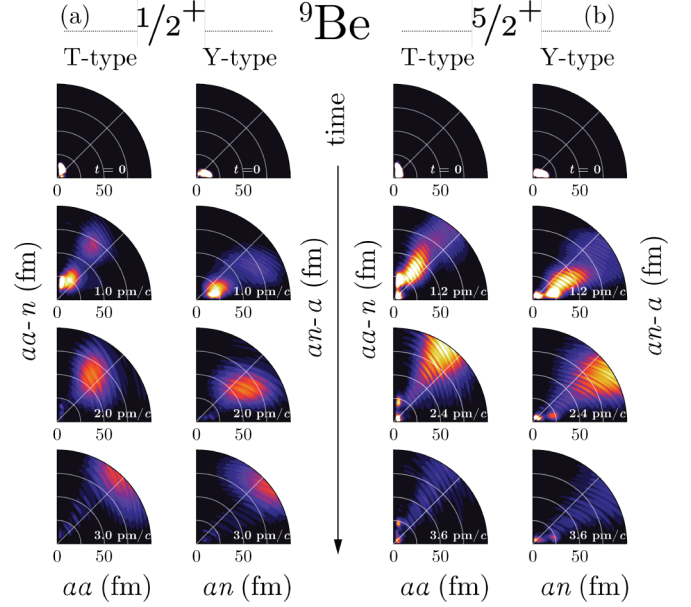


FIG. 5. Time evolution of the $1/2_1^+$ (a) and $5/2_1^+$ (b) states of ${}^9\text{Be}$. The density distributions are shown in Jacobi- T and $-Y$ coordinates for four different time slices. To show the asymptotic wave function clearly, all the particle densities (in fm^{-3}) are multiplied by the polar Jacobi coordinate ρ .

The time evolution of the $1/2_1^+$ and $5/2_1^+$ states of ${}^9\text{Be}$ have been shown in Fig. 5. For the $5/2_1^+$ state, the wave function is fairly localized inside the nucleus at the beginning ($t = 0$). When time evolves, the density distribution clearly shows two maxima for ${}^9\text{Be}$ associated with the triangular/ ${}^8\text{Be} + n$ configuration characterized by small/large relative distance between the valence neutron and ${}^8\text{Be}$ [see in Fig. 5(b)]. While tunneling, the density flux indicates that the emitted neutron is more likely to belong to the ${}^8\text{Be} + n$ branch than to the triangular component. This indicates that the valence neutron is emitted prior to the splitting of ${}^8\text{Be}$ into two α particles, which corresponds to a sequential decay process. Similar situation happens in the $3/2_1^+$ state of ${}^9\text{Be}$.

This decay mechanism can also be recognized by the asymptotic correlations of the emitted α particles. The ones from the $5/2_1^+$ state of ${}^9\text{Be}$ is shown in Fig. 6. Since the energy and angular correlations can be directly measured by the experiment, it would be useful to analyze the connection between these asymptotic observables and the decay mechanism. For a sequential decay, since the system would decay through an intermediate state of the neighboring nucleus, one may expect a pronounced peak in the energy correlations of Jacobi- T or $-Y$ coordinates. This is in accord with the situation of the $5/2_1^+$ state of ${}^9\text{Be}$, in which the energy correlation in the Jacobi- T coordinate is dominated by the peak at the region with small $E_{\alpha-\alpha}$ values. Meanwhile, due to the fact that the g.s. of ${}^8\text{Be}$ has relatively small decay energy/width, and its mass is much larger than a neutron, the neutron is preferred to carry most of the decay energy during the two-body mechanism of sequential decay. Consequently, this decay process can be roughly viewed as two independent steps, and the valence neutron has no favorable emitting

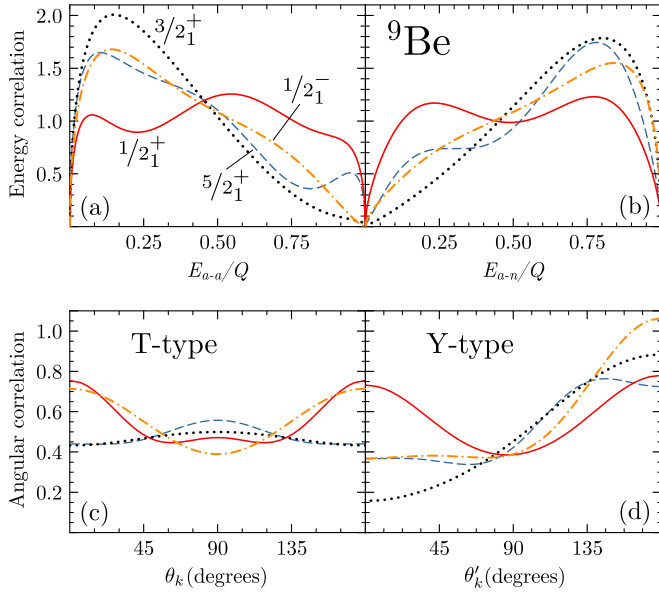


FIG. 6. Asymptotic energy (a),(b) and angular (c),(d) correlations of emitted α particles from the $1/2_1^+$ (solid lines), $3/2_1^+$ (dotted lines), $5/2_1^+$ (dashed lines), and $1/2_1^-$ (dash-dot lines) states of ${}^9\text{Be}$. Q is the total decay energy.

direction, which manifests itself as a uniform distribution of the angular correlation in the Jacobi- T coordinate approximately. Meanwhile, due to the comparable decay dynamics, the nucleon-nucleon correlation of ${}^9\text{Be}(3/2_1^+, 1/2_1^-)$ looks similar to that of ${}^9\text{Be}(5/2_1^+)$ and ${}^9\text{B}(5/2_1^+)$ (see Figs. 6 and 7).

As to the $1/2_1^+$ state of ${}^9\text{Be}$, although the wave function of the system is dominated by ${}^8\text{Be} + n$ at the initial stage, most of the tunneling process occurs from this branch. The resulting asymptotic correlations of the emitted α particles are different.

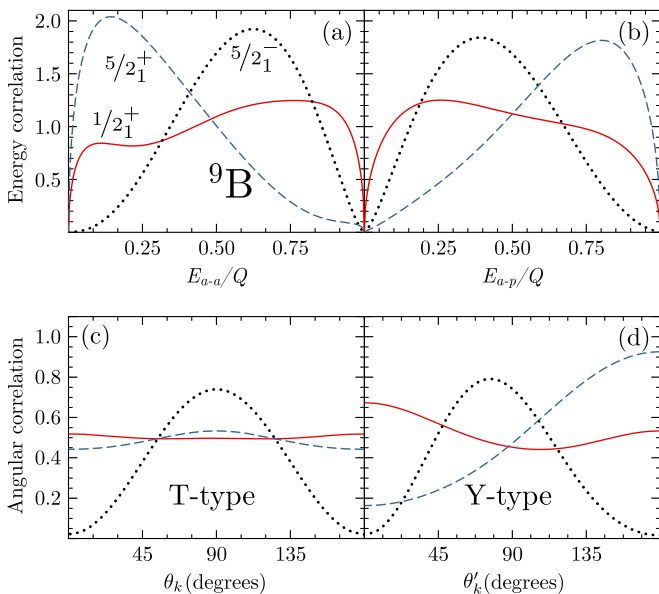


FIG. 7. Similar to Fig. 6 but for the $1/2_1^+$ (solid lines), $5/2_1^+$ (dotted lines), and $5/2_1^-$ (dashed lines) states of ${}^9\text{B}$.

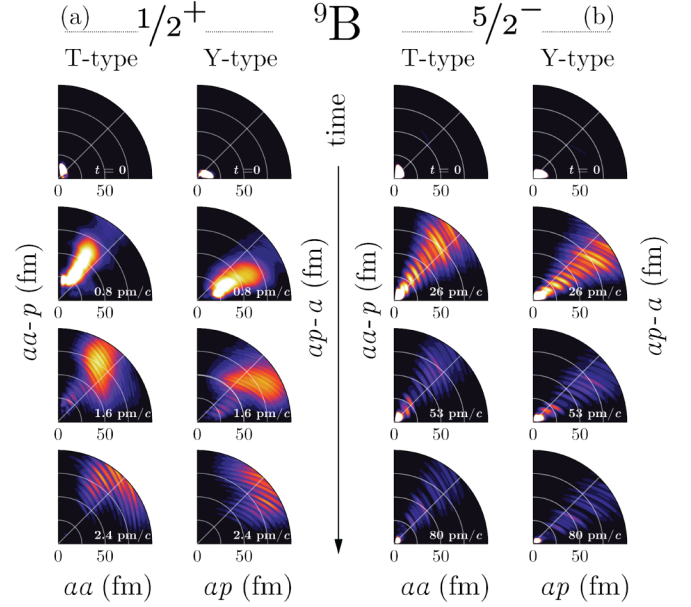


FIG. 8. Similar to Fig. 5 but for the $1/2_1^+$ (a) and $5/2_1^-$ (b) states of ${}^9\text{B}$.

The energy correlations of the $1/2_1^+$ state in both Jacobi- T and $-Y$ coordinates are more uniformly distributed, and there is no clearly preferred energy. This is probably due to the $1/2_1^+$ state being close to the threshold of $\alpha + \alpha + n$, which has a relatively small decay energy/width that is comparable with the g.s. of ${}^8\text{Be}$. Therefore, the decay process is relatively slow compared to that of the $5/2_1^+$ state. Consequently, the emission of the valence neutron is along with the breakup of ${}^8\text{Be}$, which results in a competition between sequential and three-body decay. A similar situation could be possibly referred to as the “democratic” decay mode of ${}^6\text{Be}$ [41].

Moreover, to gain more insight into the interplay between Coulomb and nuclear interactions, the decay properties of the $1/2_1^+$ states from the ${}^9\text{Be}$ and ${}^9\text{B}$ mirror pair have been compared. For most aspects, such as density evolution and energy correlation, these two analog states look similar. The main discrepancy lies in the angular correlation. Although both angular correlations are widely distributed, the small and large emitted opening angles are more favorable for the $1/2_1^+$ state of ${}^9\text{Be}$ [see Figs. 6(c) and 6(d)]. It indicates that a chain-like decay might occur, which corresponds the valence neutron being emitted from the elongation axis of the deformed ${}^8\text{Be}$. However, this decay behavior is largely suppressed in the case of ${}^9\text{B}$ due to the presence of the Coulomb interaction and the difference of the decay energies [see Figs. 7(c) and 7(d)]. This is in agreement with the conclusion of Ref. [73] that the long-range Coulomb interaction could strongly impact the angular correlation.

A possible three-body decay happens in the $5/2_1^-$ state of ${}^9\text{B}$ and ${}^9\text{Be}$ [the calculated results of them are almost the same, so only ${}^9\text{B}(5/2_1^-)$ is listed], whose initial state forms a triangular configuration. Due to the relatively large orbital-angular momentum, the structures of the two-body subsystems are largely destroyed, which results in a three-body decay process. This can be shown by the density evolution in Fig. 8, in which

most 2α particles are emitted along the 45° lines of the density distributions in Jacobi- T and $-Y$ coordinates. Moreover, the calculated energy correlation is in accordance with the experimental result of Ref. [51], in which three constituent clusters of the system share similar energies and the particles are most likely to emit with the opening angle around 90° . The relatively large orbital-angular momentum and negative parity may prevent the formation of ^8Be , which inhibit the decay of n and result in the three-body decay with small width.

IV. SUMMARY

In this work, we studied the structure and decay information of ^9Be and ^9B with the three-body GCC model. The symmetry and symmetry-breaking of these mirror systems have been compared. It has been found that, due to the different thresholds and continuum effects, the inner structures of these mirror systems can be slightly different, especially for the states with small orbital-angular momenta.

We also investigated the $1/2_1^+$ state of ^9Be whose nature is still under debate. By comparing the wave functions in the two- and three-body frameworks, we found that the behavior of the two-body virtual state can leave an imprint in a

many-body system, but its characteristics might be diluted by the configuration mixing especially for the nuclei with two subsystems unbound. To pin down the very nature of the $1/2^+$ structure, further experimental and theoretical studies, such as cross section and decay properties [92], might be required.

Moreover, the decay properties of the low-lying states of ^9Be and ^9B have been studied. The calculated energy and angular correlations of the $5/2_1^-$ state of ^9B are in good agreement with the experimental data. Further, based on the density evolution and asymptotic correlations of the emitted particles, the possible decay mechanisms have been discussed and divided into different categories.

ACKNOWLEDGMENTS

This work is partially supported by the National Key Research and Development Program (MOST Grant No. 2022YFA1602303), the National Natural Science Foundation of China (Grants No. 12147101, No. 11925502, No. 11935001, No. 11961141003, and No. 11890714), the National Key R&D Program of China (Grant No. 2018YFA0404404), the Strategic Priority Research Program of Chinese Academy of Sciences (Grant No. XDB34030000).

-
- [1] K. S. Chichak, S. J. Cantrill, A. R. Pease, S. H. Chiu, G. W. V. Cave *et al.*, Molecular Borromean rings, *Science* **304**, 1308 (2004).
- [2] Y. Aksyutina, T. Aumann, K. Boretzky, M. J. G. Borge, C. Caesar *et al.*, Momentum profile analysis in one-neutron knockout from Borromean nuclei, *Phys. Lett. B* **718**, 1309 (2013).
- [3] R. Smith, M. Freer, C. Wheldon, N. Curtis, S. Almaraz-Calderon *et al.*, Breakup branches of Borromean ^9Be , *AIP Conf. Proc.* **1681**, 060003 (2015).
- [4] P. R. Christensen and C. L. Cocke, Neutron decay of the 2.43 MeV and 3.03 MeV states in ^9Be to $^8\text{Be}(g.s.)$, *Nucl. Phys.* **89**, 656 (1966).
- [5] G. Nyman, R. E. Azuma, P. G. Hansen, B. Jonson, P. O. Larsson *et al.*, The beta decay of ^9Li to levels in ^9Be : A new look, *Nucl. Phys. A* **510**, 189 (1990).
- [6] K. Sumiyoshi, H. Utsunomiya, S. Goko, and T. Kajino, Astrophysical reaction rate for $\alpha(\alpha n, \gamma)^9\text{Be}$ by photodisintegration, *Nucl. Phys. A* **709**, 467 (2002).
- [7] P. Papka, T. A. D. Brown, B. R. Fulton, D. L. Watson, S. P. Fox *et al.*, Decay path measurements for the 2.429 MeV state in ^9Be : Implications for the astrophysical $\alpha + \alpha + n$ reaction, *Phys. Rev. C* **75**, 045803 (2007).
- [8] T. A. D. Brown, P. Papka, B. R. Fulton, D. L. Watson, S. P. Fox *et al.*, Decay studies for states in ^9Be up to 11 MeV: Insights into the $n + ^8\text{Be}$ and $\alpha + ^5\text{He}$ cluster structure, *Phys. Rev. C* **76**, 054605 (2007).
- [9] E. M. Henley and P. D. Kunz, Decay of $^9\text{Be}^*$ (2.43-MeV state), *Phys. Rev.* **118**, 248 (1960).
- [10] Y. C. Tang, F. C. Khanna, R. C. Herndon, and K. Wildermuth, ^9Be in the cluster model, *Nucl. Phys.* **35**, 421 (1962).
- [11] J. Hiura and I. Shimodaya, Alpha-particle model for ^9Be , *Prog. Theor. Phys.* **30**, 585 (1963).
- [12] R. Grubman and T. Witten, Jr., The Faddeev equations for spin-dependent forces: Calculation of ^9Be binding energy, *Nucl. Phys. A* **158**, 289 (1970).
- [13] W. Zahn, ^9Be quasibound states from a refined resonating group calculation, *Nucl. Phys. A* **269**, 138 (1976).
- [14] H. Furutani, H. Kanada, T. Kaneko, S. Nagata, H. Nishioka *et al.*, Chapter III. Study of non-alpha-nuclei based on the viewpoint of cluster correlations, *Prog. Theor. Phys. Suppl.* **68**, 193 (1980).
- [15] M. Aygun and Z. Aygun, A theoretical study on different cluster configurations of the ^9Be nucleus by using a simple cluster model, *Nucl. Sci. Tech.* **28**, 86 (2017).
- [16] Y. Kanada-En'yo and H. Horiuchi, Structure of light unstable nuclei studied with antisymmetrized molecular dynamics, *Prog. Theor. Phys. Suppl.* **142**, 205 (2001).
- [17] Y. Kanada-En'yo, H. Horiuchi, and A. Ono, Structure of Li and Be isotopes studied with antisymmetrized molecular dynamics, *Phys. Rev. C* **52**, 628 (1995).
- [18] M. Hirai, S. Kumano, K. Saito, and T. Watanabe, Clustering aspects in nuclear structure functions, *Phys. Rev. C* **83**, 035202 (2011).
- [19] Y. Kanada-En'yo, Isovector and isoscalar dipole excitations in ^9Be and ^{10}Be studied with antisymmetrized molecular dynamics, *Phys. Rev. C* **93**, 024322 (2016).
- [20] K. Arai, P. Descouvemont, D. Baye, and W. N. Catford, Resonance structure of ^9Be and ^9B in a microscopic cluster model, *Phys. Rev. C* **68**, 014310 (2003).
- [21] V. S. Vasilevsky, K. Katō, and N. Zh. Takibayev, Formation and decay of resonance states in ^9Be and ^9B nuclei: Microscopic three-cluster model investigations, *Phys. Rev. C* **96**, 034322 (2017).
- [22] M. Bouten, M. C. Bouten, H. Depuydt, and L. Schotsmans, Projected Hartree-Fock calculations for light nuclei:

- (IV). Normal parity states of ${}^9\text{Be}$, *Nucl. Phys. A* **127**, 177 (1969).
- [23] F. C. Barker, Intermediate coupling shell-model calculations for light nuclei, *Nucl. Phys.* **83**, 418 (1966).
- [24] V. Della Rocca and F. Iachello, Cluster shell model: I. Structure of ${}^9\text{Be}$, ${}^9\text{B}$, *Nucl. Phys. A* **973**, 1 (2018).
- [25] S. C. Pieper, K. Varga, and R. B. Wiringa, Quantum Monte Carlo calculations of $A = 9, 10$ nuclei, *Phys. Rev. C* **66**, 044310 (2002).
- [26] C. Fors sen, P. Navr til, W. E. Ormand, and E. Caurier, Large basis ab initio shell model investigation of ${}^9\text{Be}$ and ${}^{11}\text{Be}$, *Phys. Rev. C* **71**, 044312 (2005).
- [27] B. S. Huang and Y. G. Ma, Dipole excitation of ${}^6\text{Li}$ and ${}^9\text{Be}$ studied with an extended quantum molecular dynamics model, *Phys. Rev. C* **103**, 054318 (2021).
- [28] C. Z. Shi and Y. G. Ma, Alpha-clustering effect on flows of direct photons in heavy-ion collisions, *Nucl. Sci. Tech.* **32**, 66 (2021).
- [29] W. B. He, Y. G. Ma, X. G. Cao, X. Z. Cai, and G. Q. Zhang, Giant dipole resonance as a fingerprint of α clustering configurations in ${}^{12}\text{C}$ and ${}^{16}\text{O}$, *Phys. Rev. Lett.* **113**, 032506 (2014).
- [30] V. D. Eftros and J. M. Bang, The first excited states of ${}^9\text{Be}$ and ${}^9\text{B}$, *Eur. Phys. J. A* **4**, 33 (1999).
- [31] M. Odsuren, Y. Kikuchi, T. Myo, M. Aikawa, and K. Kat o, Virtual-state character of the ${}^9\text{Be}(1/2^+)$ state in the ${}^9\text{Be}(\gamma, n){}^8\text{Be}$ reaction, *Phys. Rev. C* **92**, 014322 (2015).
- [32] E. Garrido, D. V. Fedorov, and A. S. Jensen, Above threshold s-wave resonances illustrated by the $1/2^+$ states in ${}^9\text{Be}$ and ${}^9\text{B}$, *Phys. Lett. B* **684**, 132 (2010).
- [33] R.  lvarez-Rodr guez, A. S. Jensen, E. Garrido, and D. V. Fedorov, Structure and three-body decay of ${}^9\text{Be}$ resonances, *Phys. Rev. C* **82**, 034001 (2010).
- [34] V. D. Eftros, P. von Neumann-Cosel, and A. Richter, Properties of the first excited state of ${}^9\text{Be}$ derived from (γ, n) and (e, e') reactions, *Phys. Rev. C* **89**, 027301 (2014).
- [35] G. Kuechler, A. Richter, and W. von Witsch, Line shape and excitation strength of the first excited state in ${}^9\text{Be}$, *Eur. Phys. J. A* **326**, 447 (1987).
- [36] L. G. Sobotka and M. Piarulli, Collisions hint that four neutrons form a transient isolated entity, *Nature (London)* **606**, 656 (2022).
- [37] J. Casal, M. Rodr guez-Gallardo, J. M. Arias, and I. J. Thompson, Astrophysical reaction rate for ${}^9\text{Be}$ formation within a three-body approach, *Phys. Rev. C* **90**, 044304 (2014).
- [38] M. Pf tznern, M. Karny, L. V. Grigorenko, and K. Riisager, Radioactive decays at limits of nuclear stability, *Rev. Mod. Phys.* **84**, 567 (2012).
- [39] B. Blank and M. Ploszajczak, Two-proton radioactivity, *Rep. Prog. Phys.* **71**, 046301 (2008).
- [40] J. Giovinazzo, B. Blank, M. Chartier, S. Czajkowski, A. Fleury *et al.*, Two-proton radioactivity of ${}^{45}\text{F}$, *Phys. Rev. Lett.* **89**, 102501 (2002).
- [41] I. A. Egorova, R. J. Charity, L. V. Grigorenko, Z. Chajecski, D. Coupland *et al.*, Democratic decay of ${}^6\text{Be}$ exposed by correlations, *Phys. Rev. Lett.* **109**, 202502 (2012).
- [42] L. Zhou, S. M. Wang, D. Q. Fang, and Y. G. Ma, Recent progress in two-proton radioactivity, *Nucl. Sci. Tech.* **33**, 105 (2022).
- [43] Y. G. Ma, D. Q. Fang, X. Y. Sun, P. Zhou, Y. Togano *et al.*, Different mechanism of two-proton emission from proton-rich nuclei ${}^{23}\text{Al}$ and ${}^{22}\text{Mg}$, *Phys. Lett. B* **743**, 306 (2015).
- [44] D. X. Zhu, Y. Y. Xu, H. M. Liu, X. J. Wu, B. He *et al.*, Two-proton radioactivity of the excited state within the Gamow-like and modified Gamow-like models, *Nucl. Sci. Tech.* **33**, 122 (2022).
- [45] M. Pf tznern, I. Mukha, and S. M. Wang, Two-proton emission and related phenomena, *Prog. Part. Nucl. Phys.* **132**, 104050 (2023).
- [46] S. M. Wang, W. Nazarewicz, R. J. Charity, and L. G. Sobotka, Nucleon-nucleon correlations in the extreme oxygen isotopes, *J. Phys. G* **49**, 10LT02 (2022).
- [47] Z. Kohley, T. Baumann, D. Bazin, G. Christian, P. A. DeYoung *et al.*, Study of two-neutron radioactivity in the decay of ${}^{26}\text{O}$, *Phys. Rev. Lett.* **110**, 152501 (2013).
- [48] A. Spyrou, Z. Kohley, T. Baumann, D. Bazin, B. A. Brown *et al.*, First observation of ground state dineutron decay: ${}^{16}\text{Be}$, *Phys. Rev. Lett.* **108**, 102501 (2012).
- [49] Z. Kohley, E. Lunderberg, P. A. DeYoung, A. Volya, T. Baumann *et al.*, First observation of the ${}^{13}\text{Li}$ ground state, *Phys. Rev. C* **87**, 011304(R) (2013).
- [50] Y. Liu and Y. L. Ye, Nuclear clustering in light neutron-rich nuclei, *Nucl. Sci. Tech.* **29**, 184 (2018).
- [51] R. J. Charity, J. M. Elson, J. Manfredi, R. Shane, L. G. Sobotka *et al.*, Investigations of three-, four-, and five-particle decay channels of levels in light nuclei created using a ${}^9\text{C}$ beam, *Phys. Rev. C* **84**, 014320 (2011).
- [52] R. G. Thomas, An analysis of the energy levels of the mirror nuclei, ${}^{13}\text{C}$ and ${}^{13}\text{N}$, *Phys. Rev.* **88**, 1109 (1952).
- [53] J. B. Ehrman, On the displacement of corresponding energy levels of ${}^{13}\text{C}$ and ${}^{13}\text{N}$, *Phys. Rev.* **81**, 412 (1951).
- [54] S. M. Wang, W. Nazarewicz, R. J. Charity, and L. G. Sobotka, Structure and decay of the extremely proton-rich nuclei ${}^{11,12}\text{O}$, *Phys. Rev. C* **99**, 054302 (2019).
- [55] S. Zhang, Y. Z. Ma, J. G. Li, B. S. Hu, Q. Yuan *et al.*, The roles of three-nucleon force and continuum coupling in mirror symmetry breaking of oxygen mass region, *Phys. Lett. B* **827**, 136958 (2022).
- [56] S. Zhang, F. R. Xu, J. G. Li, B. S. Hu, Z. H. Cheng *et al.*, Ab initio descriptions of $A = 16$ mirror nuclei with resonance and continuum coupling, [arXiv:2301.01951](https://arxiv.org/abs/2301.01951) [nucl-th].
- [57] S. M. Wang, N. Michel, W. Nazarewicz, and F. R. Xu, Structure and decays of nuclear three-body systems: The Gamow coupled-channel method in Jacobi coordinates, *Phys. Rev. C* **96**, 044307 (2017).
- [58] T. Berggren, On the use of resonant states in eigenfunction expansions of scattering and reaction amplitudes, *Nucl. Phys. A* **109**, 265 (1968).
- [59] N. Michel, W. Nazarewicz, M. Ploszajczak, and K. Bennaceur, Gamow shell model description of neutron-rich nuclei, *Phys. Rev. Lett.* **89**, 042502 (2002).
- [60] G. Gamow, Zur quantentheorie des atomkernes, *Z. Phys.* **51**, 204 (1928).
- [61] I. M. Gel'fand and N. Y. Vilenkin, *Generalized Functions* (Academic Press, New York, 1961).
- [62] J.-P. Antoine, R. C. Bishop, A. Bohm, and S. Wickramasekara, *Rigged Hilbert Spaces in Quantum Physics*, Compendium of Quantum Physics (Compendium of Quantum Physics. Springer, Berlin/Heidelberg, 2009), pp. 640–650.
- [63] I. J. Thompson, B. V. Danilin, V. D. Eftros, J. S. Vaagen, J. M. Bang, and M. V. Zhukov, Pauli blocking in three-body models of halo nuclei, *Phys. Rev. C* **61**, 024318 (2000).

- [64] I. J. Thompson, F. M. Nunes, and B. V. Danilin, FaCE: A tool for three body Faddeev calculations with core excitation, *Comput. Phys. Commun.* **161**, 87 (2004).
- [65] P. Descouvemont, C. Daniel, and D. Baye, Three-body systems with Lagrange-mesh techniques in hyperspherical coordinates, *Phys. Rev. C* **67**, 044309 (2003).
- [66] K. Wildermuth and Y. C. Tang, *A Unified Theory of the Nucleus* (Academic Press, New York, 1977).
- [67] S. M. Wang, J. C. Pei, and F. R. Xu, Spectroscopic calculations of cluster nuclei above double shell closures with a new local potential, *Phys. Rev. C* **87**, 014311 (2013).
- [68] B. Buck, A. C. Merchant, and S. M. Perez, Systematics of alpha-cluster states above double shell closures, *Phys. Rev. C* **51**, 559 (1995).
- [69] B. Buck, H. Friedrich, and C. Wheatley, Local potential models for the scattering of complex nuclei, *Nucl. Phys. A* **275**, 246 (1977).
- [70] N. Michel and M. Płoszajczak, *Gamow Shell Model, The Unified Theory of Nuclear Structure and Reactions*, Lecture Notes in Physics, Vol. 983 (Springer, Cham, 2021).
- [71] N. Michel, W. Nazarewicz, M. Płoszajczak, and J. Okołowicz, Gamow shell model description of weakly bound nuclei and unbound nuclear states, *Phys. Rev. C* **67**, 054311 (2003).
- [72] N. Michel, W. Nazarewicz, M. Płoszajczak, and T. Vertse, Shell model in the complex energy plane, *J. Phys. G* **36**, 013101 (2009).
- [73] S. M. Wang and W. Nazarewicz, Fermion pair dynamics in open quantum systems, *Phys. Rev. Lett.* **126**, 142501 (2021).
- [74] A. I. Baz', Y. B. Zel'dovich, and A. M. Perelomov, *Scattering, Reactions and Decay in Nonrelativistic Quantum Mechanics* (Israel Program for Scientific Translation, Jerusalem, 1969).
- [75] A. Volya, Time-dependent approach to the continuum shell model, *Phys. Rev. C* **79**, 044308 (2009).
- [76] Y. Kikuchi, M. Odsuren, T. Myo, and K. Katō, Photodisintegration cross section of ${}^9\text{Be}$ up to 16 MeV in the $\alpha + \alpha + n$ three-body model, *Phys. Rev. C* **93**, 054605 (2016).
- [77] H. Kanada, T. Kaneko, S. Nagata, and M. Nomoto, Microscopic study of nucleon- ${}^4\text{He}$ scattering and effective nuclear potentials, *Prog. Theor. Phys.* **61**, 1327 (1979).
- [78] E. W. Schmid and K. Wildermuth, Phase shift calculations on $\alpha - \alpha$ scattering, *Nucl. Phys.* **26**, 463 (1961).
- [79] D. R. Tilley, J. H. Kelley, J. L. Godwin, D. J. Millener, J. E. Purcell *et al.*, Energy levels of light nuclei $A = 8, 9, 10$, *Nucl. Phys. A* **745**, 155 (2004).
- [80] F. Ajzenberg-Selove, Energy levels of light nuclei $A = 5-10$, *Nucl. Phys. A* **490**, 1 (1988).
- [81] R. Sherr and G. Bertsch, Coulomb energy systematics and the missing $J^\pi = (1/2)^+$ state in ${}^9\text{B}$, *Phys. Rev. C* **32**, 1809 (1985).
- [82] M. Odsuren, Y. Kikuchi, T. Myo, M. Aikawa, and K. Katō, The first unbound states of mirror ${}^9\text{Be}$ and ${}^9\text{B}$ nuclei, *EPJ Web Conf.* **146**, 12012 (2017).
- [83] A. V. Nesterov, V. S. Vasilevsky, and T. P. Kovalenko, Nature of resonance states in the ${}^9\text{Be}$ and ${}^9\text{B}$ mirror nuclei, *Phys. At. Nucl.* **77**, 555 (2014).
- [84] R. Álvarez-rodríguez, A. S. Jensen, D. V. Fedorov, and E. Garrido, Momentum distributions from three-body decaying ${}^9\text{Be}$ and ${}^9\text{B}$ resonances, *Int. J. Mod. Phys. E* **20**, 827 (2011).
- [85] Evaluated Nuclear Structure Data File (ENSDF), <http://www.nndc.bnl.gov/ensdf/>.
- [86] M. A. Tiede, K. W. Kemper, N. R. Fletcher, D. Robson, D. D. Caussyn *et al.*, Measurement of low-lying states in ${}^9\text{B}$, *Phys. Rev. C* **52**, 1315 (1995).
- [87] F. C. Barker, Energies of ${}^9\text{B}(1/2^+)$ and ${}^{10}\text{C}(0_2^+)$, *Phys. Rev. C* **79**, 017302 (2009).
- [88] F. C. Barker, Energy of the first excited state of ${}^9\text{B}$, *Phys. Rev. C* **53**, 2539 (1996).
- [89] H. T. Fortune, $1d_{5/2}-2s_{1/2}$ splitting in light nuclei, *Phys. Rev. C* **52**, 2261 (1995).
- [90] H. T. Fortune and R. Sherr, Constraints on energy of ${}^9\text{B}(1/2^+)$ and ${}^{10}\text{C}(0_2^+)$, *Phys. Rev. C* **73**, 064302 (2006).
- [91] H. Utsunomiya, S. Katayama, I. Gheorghe, S. Imai, H. Yamaguchi *et al.*, Photodisintegration of ${}^9\text{Be}$ through the $1/2^+$ state and cluster dipole resonance, *Phys. Rev. C* **92**, 064323 (2015).
- [92] S. M. Wang, W. Nazarewicz, A. Volya, and Y. G. Ma, Probing the nonexponential decay regime in open quantum systems, *Phys. Rev. Res.* **5**, 023183 (2023).